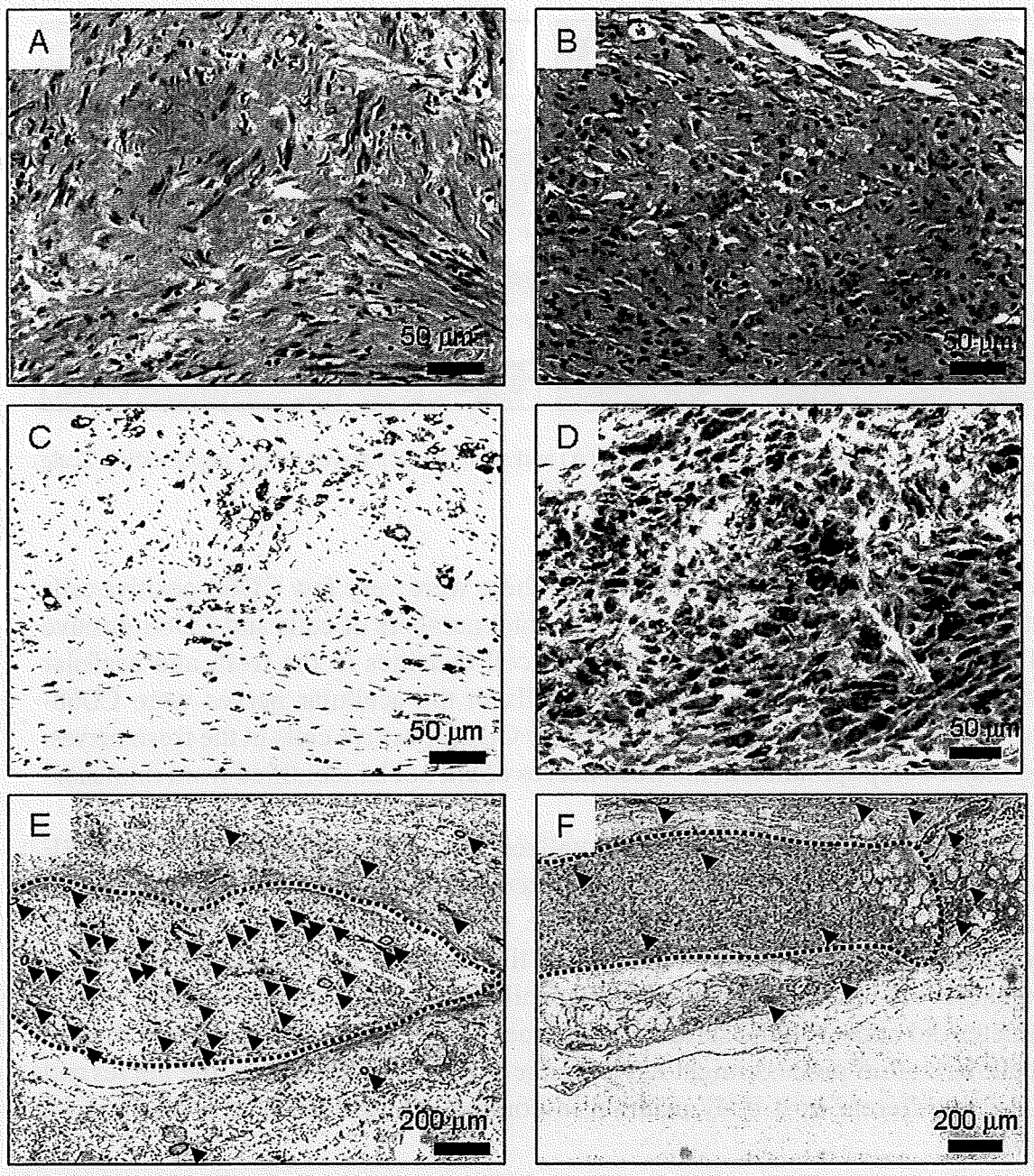

Figure 3. HE staining (A, B) and immunostaining for CD68 (C, D) and vWF (E, F) in subcutaneously implanted allogeneic fresh (A, C, E) and allogeneic acellular (B, D, F) nerves 1 month postimplantation. The images of HE staining and immunostaining for CD68 show the middle areas of the implant. The dotted lines and arrowheads in E and F indicate the edge of the grafts and microvessels, respectively. This figure is published in colour in the online edition of this journal, that can be accessed *via* http://www.brill.nl/jbs

a few GFAP-positive cells with fiber-like morphologies were observed in autologous fresh nerves but not in the allogeneic acellular graft. At 158 days after the time of transplantation, both grafts showed a fiber-like formation of GFAP-positive cells. At that time point, the acellular grafts included cells with thinner fiber-like morphology than the fresh nerves.

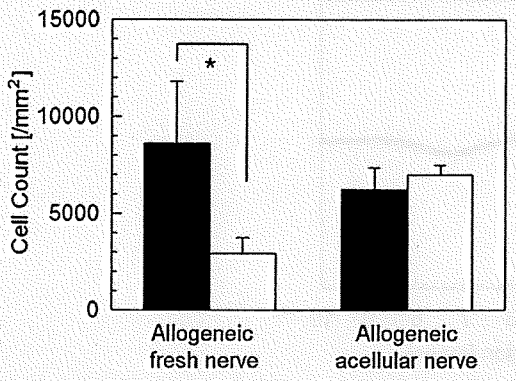

Figure 4. Number of total infiltrated cells (black column) and macrophages (white column) in the allogeneic fresh and allogeneic acellular nerves at 1-month postoperation ($n = 3$ each). Three magnified pictures were taken in each graft and the cells were counted. All data are indicated as the mean ± SD. *CD68-positive cells *vs* total cells in the fresh nerve $P > 0.05$.

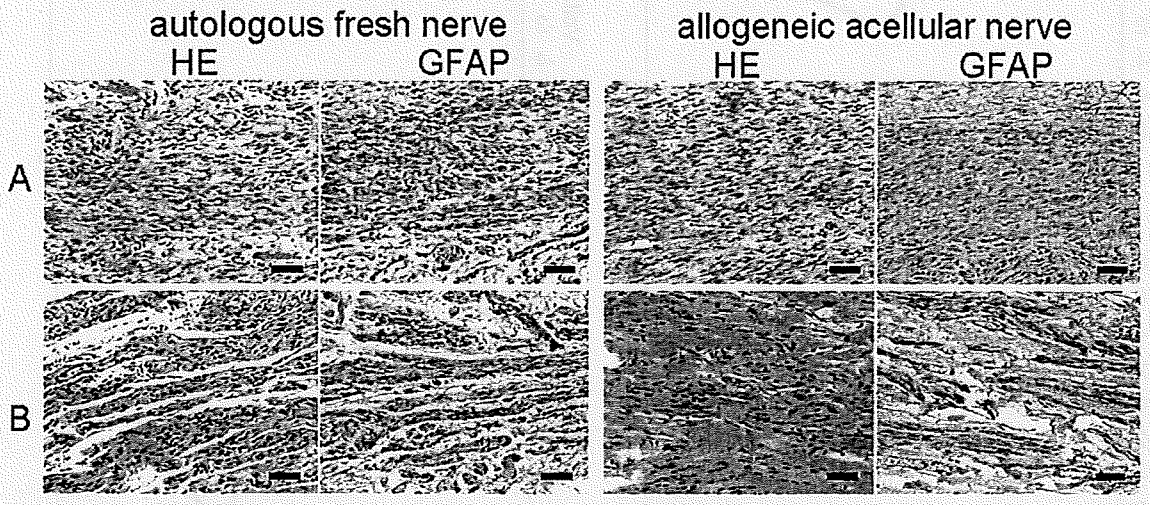

Figure 5. HE staining and immunostaining for GFAP of transplanted autologous fresh nerve and allogeneic acellular nerve (A) 110 days and (B) 158 days after operation. Scale bars = 50 μm. This figure is published in colour in the online edition of this journal, that can be accessed *via* http://www.brill.nl/jbs

3.4. Electrophysiology

Electrophysiological recovery of the allogeneic acellular nerves and autologous fresh nerves was assessed by measuring the myogenic potential of the tibial muscle group. The results from all animals subjected to the electrophysiological study are shown in Fig. 6. In the case of the autologous fresh nerves, an electrophysiological response at the tibial muscles was observed after short-term transplantation, but no reaction was seen in the acellular nerve grafts. After long-term transplantation, the electrophysiological responses in the allogeneic acellular nerve group were dramatically recovered; that is, 2 of the 3 cases showed normal reactions to the sciatic nerve stimulus (Fig. 6C). In the autologous fresh nerve group as well, only 2 of the 3 cases reacted normally to electrical stimulation. These results demonstrate that a 10-mm gap in the rat sciatic nerves can be bridged using CIP-treated allo-

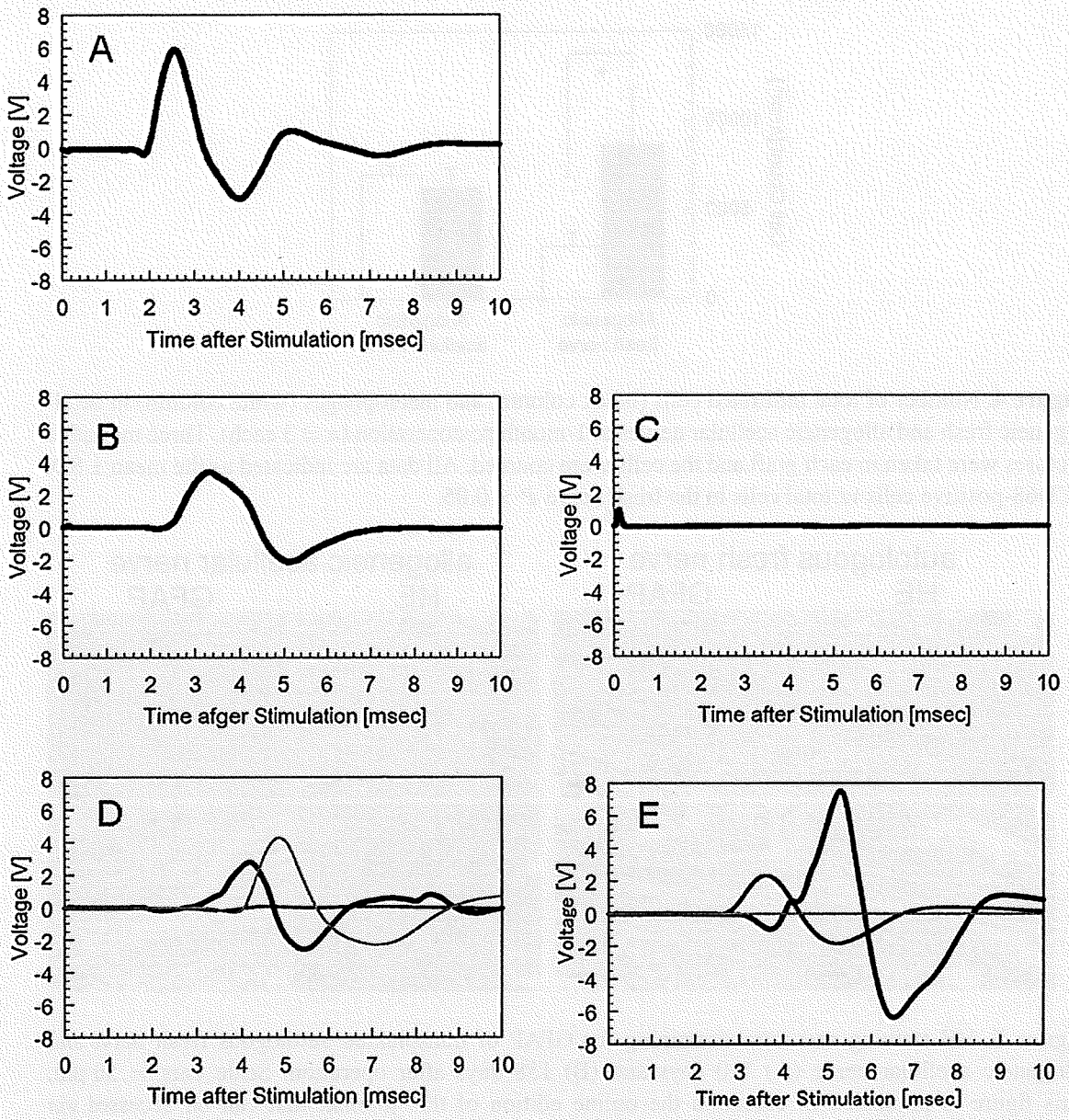

Figure 6. Averaged electromyograms of the tibial muscle of legs into which autologous fresh nerves (B, D) and allogeneic acellular nerves (C, E) were transplanted. Electromyograms before operation (A), after short-term transplantation (B, C; $n = 1$) and after long-term transplantation (D, E; $n = 3$).

geneic acellular nerves. The induced axon in that graft successfully recovered the nerve function, although the axonal growth took more time than the autologous fresh nerve did. Our results show that the myogenic potential that had completely disappeared immediately after graft transplantation was recovered thereafter.

4. Discussion

To overcome the donor shortage for peripheral nerve treatments, allogeneic acellular nerves will likely be the most viable graft for growing axons. However, there

have been only a few studies that used allogeneic animal models. In some cases, inadequate transplantation models in dogs or rats were defined as allogeneic systems [31, 33]. Rats are thought to be the best animals for investigating allogeneic transplantation because of their well-defined histocompatibility and disparity.

CIP treatment can only disrupt the cells. From this point of view, the thermal pretreatment of nerves, which is commonly used to reduce their immunogenicity, can provide the same results as our CIP treatment. However, by combining the CIP treatment with a washing process, all cells were effectively removed from the tissue. The chemical process which is commonly employed to decellularize tissue involves detergent, and that affects axonal growth. However, our washing solution did not have any such harmful component.

Electrophysiological recovery in the acellular grafts was not demonstrated in the short-term (about 5 months post-operation). It is believed that this delay of physiological recovery was caused by immature Schwann cell alignments. Although the Schwann cell alignments were observed in the acellular nerve graft 5 months after the transplantation just as in the autograft, the cells in the acellular nerve were smaller and less mature than those in the autograft. In general, from the first day to the first week following the peripheral nerve injury, macrophages are recruited in significant numbers to degenerate the axons and to remove the myelin debris for nerve regeneration. After that, the Schwann cells usually align to form pathways for the growth of axons from the proximal to distal stump of the nerve defect [34]. Thus, we evaluated the host reaction against the transplanted acellular nerves 4 weeks after implantation, since the normal reaction to injured host nerves is considered to be complete at this time point. Four weeks after the subcutaneous implantation of fresh nerves, many host cells but very few macrophages were observed in the fresh nerves (Fig. 3A and 3C), suggesting that all allogeneic cells in the transplanted nerves were removed within 1 month and replaced with the host cells. In contrast, the acellular nerves were filled with macrophages even though they did not contain any allogeneic cells when transplanted. This macrophage infiltration did not result from the incomplete removal of allogeneic cells but might have resulted from the alteration of extracellular matrix protein by CIP treatment. In fact, when the fresh and acellular nerves of SD rats were implanted in SD rats subcutaneously (isogenic transplantation), the same host reactions as in the case of the allogeneic model occurred (data not shown). It has been reported that treatment of bacteriochlorophyll with a high pressure of 0.6 GPa changed the 800-nm absorbance, reflecting a tertiary structure alteration of the protein [35]. Thus, the 980 MPa pressure used in our CIP treatment might affect the extracellular matrix structure of both allogeneic and isogenic nerves, causing them to have a much stronger foreign body reaction than that in the fresh nerve implantation. Such a large effect of CIP treatment on the ECM protein was not observed in the case of decellularization of blood vessels or cardiac valves. ECM of nerve tissue is considered to be less stable against high pressure than the fibrillar ECM of blood vessels due to the large amount of proteoglycans. Therefore, although the acellular vessels or cardiac valves prepared

by CIP treatment succeeded in tissue regeneration in animal experiments, further optimization of the CIP conditions will be needed for the nerve regeneration.

Angiogenesis is one of the inflammatory responses in material implantation. In the subcutaneous implantation study, only a low level of angiogenesis was observed in the allogeneic acellular nerves, even though many macrophages were present (Fig. 3D and 3F). On the other hand, many small vessels were observed in the allogeneic fresh nerves (Fig. 3E). We considered that the allogeneic cells were removed and host fibroblasts migrated to form granulation tissue, and then the new blood vessels were induced to provide nutritional support for these cells. In fact, different cell morphologies were observed in each of the implanted nerves (Fig. 3A and 3B). The HE staining of the allogeneic fresh nerves showed fibroblast-like cell infiltration and scar-like collagenous tissue formation in the implanted nerves, which was not observed in the acellular nerve. From these results, our acellular nerves will be suitable for nerve regeneration, even though their axonal growth was slower than that in autologous fresh nerves.

The topographical cues of nerve conduit are another important factor to be considered. A number of studies have described that the interactions between a 3-D extracellular microenvironment and axons influence neuronal growth [36]. A suitable pore size of the nerve conduits facilitates nerve regeneration. One report has shown that a macroporous synthetic nerve conduit made from poly(ε-caprolactone) with pore sizes of 1–10 μm was most effective in nerve regeneration among the bigger and smaller pore size conduits [37]. From the SEM observations, our acellular nerve had about 10 μm spaces among the remaining fibers, but failed to recover myogeneic potential even at 5 months post-operation. On the other hand, the detergent-treated allogeneic acellular nerves implanted in the 10-mm gap of a rat sciatic nerve succeeded in promoting axonal growth to the distal portion and showed good motor function, measured as electromyographic activity, within one month after the operation [20]. These good results might have arisen from the fact that their detergent-treated acellular nerves contained larger pores (20–100 μm) than our acellular nerves did. In a series of *in vitro* experiments using PC12 cells on various microchannels, Mahoney *et al.* showed that the effective widths in the neurite direction along the axis of the grooves were 20–30 μm [38]. There is expected to be a slight difference in either synthetic or tissue-derived materials between *in vivo* and *in vitro* studies. The filament diameter in the acellular nerves also affects the axonal growth activity. The optimal polypropylene filament diameter for alignment of dorsal root ganglion (DRG) neurites and outgrowth of Schwann cells has been reported to be 5 μm [39]. The combination of biomolecules with acellular nerves is expected to be another way to accelerate axonal growth. Rat acellular nerve allografts loaded with vascular endothelial growth factor and beta-nerve growth factor are reported to lead to greater axonal density at the distal portion of the graft [20].

5. Conclusion

Our allogeneic acellular nerves show promise for use as axonal scaffolds in peripheral nerve defects. As compared to allogeneic fresh nerves, the allogeneic acellular nerves did not induce scar formation in the graft, and led to a successful recovery of sciatic nerve function. Further optimization of the CIP treatment will result in fewer protein structural changes and an improvement of the spaces among the fibrous components, which may improve the regeneration rate and axon density.

Acknowledgements

This work was financially supported by a Grant-in-Aid for Young Scientists (B), a Grant-in-Aid for Scientific Research from the Ministry of Health, Labour and Welfare of Japan, and a CREST-JST grant.

References

1. J. R. Hess, M. J. Brenner, I. K. Fox, C. M. Nichols, T. M. Myckatyn, D. A. Hunter, S. R. Rickman and S. E. Mackinnon, *Plast. Reconstr. Surg.* **119**, 246 (2007).
2. D. Neubauer, J. B. Graham and D. Muir, *Exp. Neurol.* **207**, 163 (2007).
3. A. K. Gulati, *J. Neurosurg.* **68**, 117 (1988).
4. S. M. Hall, *Neuropathol. Appl. Neurobiol.* **12**, 401 (1986).
5. C. Ide, K. Tohyama, E. Yokota, T. Nitatori and S. Onodera, *Brain Res.* **288**, 61 (1983).
6. S. E. Mackinnon, V. B. Doolabh, C. B. Novak and E. P. Trulock, *Plast. Reconstr. Surg.* **107**, 1419 (2001).
7. M. Sondell, G. Lundborg and M. Kanje, *Brain Res.* **795**, 44 (1998).
8. T. W. Hudson, S. Zawko, C. Deister, S. Lundy, C. Y. Hu, K. Lee and C. E. Schmidt, *Tissue Eng.* **10**, 1641 (2004).
9. B. Hontanilla, C. Audá, J. Aucocha and O. Gorría, *Neurosurgery* **58**, 768 (2006).
10. C. B. Jenq and R. E. Coggeshall, *Brain Res.* **361**, 233 (1985).
11. T. M. Myckatyn and S. E. Mackinnon, *Neurol. Res.* **26**, 124 (2004).
12. T. Osawa, C. Ide and K. Tohyama, *Arch. Histol. Jpn* **50**, 193 (1987).
13. P. J. Evans, R. Midha and S. E. Mackinnson, *Prog. Neurobiol.* **43**, 187 (1994).
14. Z. Li, J. Peng, G. Wang, Q. Yang, H. Yu, Q. Guo, A. Wang, B. Zhao and S. Lu, *Exp. Neurol.* **214**, 47 (2008).
15. A. K. Gulati and G. P. Cole, *J. Neurosurg.* **72**, 114 (1990).
16. N. Danielsen, J. M. Kerns, B. Holmquist, Q. Zhao, G. Lundborg and M. Kanje, *Brain Res.* **681**, 105 (1995).
17. T. W. Hudson, S. Y. Liu and C. E. Schmidt, *Tissue Eng.* **10**, 1346 (2004).
18. T. Osawa, K. Tohyama and C. Ide, *J. Neurocytol.* **19**, 833 (1990).
19. J. Sørensen, K. Fugleholm, M. Moldovan, H. Schmalbruch and C. Krarup, *Brain Res.* **903**, 185 (2001).
20. B. S. Kim, J. J. Yoo and A. Atala, *J. Biomed. Mater. Res. A* **68**, 201 (2004).
21. J. M. Rovak, D. K. Bishop, L. K. Boxer, S. C. Wood, A. K. Mungara and P. S. Cederna, *J. Reconstr. Microsurg.* **21**, 207 (2005).
22. H. C. Ott, T. S. Matthiesen, S. K. Goh, L. D. Black, S. M. Kren, T. I. Netoff and D. A. Taylor, *Nature Med.* **14**, 213 (2008).

23. S. R. Meyer, J. Nagendran, L. S. Desai, G. R. Rayat, T. A. Churchill, C. C. Anderson, R. V. Rajotte, J. R. Lakey and D. B. Ross, *J. Thorac. Cardiovasc. Surg.* **130**, 469 (2005).
24. S. Mirsadraee, H. E. Wilcox, K. G. Watterson, J. N. Kearney, J. Hunt, J. Fisher and E. Ingham, *J. Surg. Res.* **143**, 407 (2007).
25. C. Ide, T. Osawa and K. Tohyama, *Prog. Neurobiol.* **34**, 1 (1990).
26. S. E. Mackinnon, A. R. Hudson, R. E. Falk, D. Kline and D. Hunter, *Neurosurgery* **15**, 690 (1984).
27. E. L. Whitlock, S. H. Tuffaha, J. P. Luciano, Y. Yan, D. A. Hunter, C. K. Magill, A. M. Moore, A. Y. Tong, S. E. Mackinnon and G. H. Borschel, *Muscle Nerve* **39**, 787 (2009).
28. T. Fujisato, K. Minatoya, S. Yamazaki, Y. Meng, K. Niwaya, A. Kishida, T. Nakatani and S. Kitamura, in: *Cardiovascular Regeneration Therapies Using Tissue Engineering Approaches*, H. Mori and H. Matsuda (Eds), p. 83. Springer, Tokyo (2005).
29. S. Hall, *J. Anat.* **190**, 57 (1997).
30. G. Keilhoff, F. Prätsch, G. Wolf and H. Fansa, *Tissue Eng.* **11**, 1004 (2005).
31. C. Ide, K. Tohyama, K. Tajima, K. Endoh, K. Sano, M. Tamura, A. Mizoguchi, M. Kitada, T. Morihara and M. Shirasu, *Exp. Neurol.* **154**, 99 (1998).
32. P. J. Evans, S. E. Mackinnon, R. Midha, J. A. Wade, D. A. Hunter, Y. Nakao and G. M. T. Hare, *Microsurgery* **19**, 115 (1999).
33. M. Nakamura, N. Tomizawa, K. Tohyama and S. Hara, *J. Vet. Med. Sci.* **66**, 767 (2004).
34. V. H. Perry, M. C. Brown and S. Gordon, *J. Exp. Med.* **165**, 1218 (1987).
35. A. Gall, A. Ellervee, J. N. Sturgis, N. J. Fraser, R. J. Cogdell, A. Freiberg and B. Robert, *Biochemistry* **42**, 13019 (2003).
36. G. N. Li and D. Hoffman-Kim, *Tissue Eng.* **14**, 33 (2008).
37. C. L. A. M. Vleggeert-Lankanp, G. C. W. de Ruiter, J. F. C. Wolfs, A. P. Pêgo, R. J. van den Berg, H. K. P. Feirabend, M. J. A. Malessy and E. A. J. F. Lakke, *J. Biomed. Mater. Res. A* **80**, 965 (2007).
38. M. J. Mahoney, R. R. Chen, J. Tan and W. M. Saltzman, *Biomaterials* **26**, 771 (2005).
39. X. Wen and P. A. Tresco, *J. Biomed. Mater. Res. A* **76**, 626 (2006).

Received: 11 August 2009, Revised: 1 April 2010, Accepted: 8 April 2010, Published online in Wiley InterScience: 00 Month 2010

(www.interscience.wiley.com) DOI:10.1002/cmmi.389

Design and characterization of a polymeric MRI contrast agent based on PVA for *in vivo* living-cell tracking

Yoichi Tachibana[a], Jun-ichiro Enmi[b], Atsushi Mahara[a], Hidehiro Iida[b] and Tetsuji Yamaoka[a]*

A novel water-soluble MRI contrast agent for *in vivo* living cell tracking was developed. Unlike the conventional *in vivo* cell tracking system based on superparamagnetic iron oxide beads, the newly developed contrast agent is eliminated from the body when the contrast agent exits the cells upon cell death, which makes living cell tracking possible. The contrast agent is composed of gadolinium chelates (Gd-DOTA) and a water-soluble carrier, poly(vinyl alcohol) (PVA), which is known to interact with cells and tissues very weakly. Since the Gd-PVA was not taken up by cells spontaneously, the electroporation method was used for cell labeling. The delivered Gd-PVA was localized only in the cytosolic compartment of growing cells with low cytotoxicity and did not leak out of the living cells for long periods of time. This stability may be due to the weak cell-membrane affinity of Gd-PVA, and did not affect cell proliferation at all. After cell labeling, signal enhancement of cells was observed *in vitro* and *in vivo*. These results indicate that Gd-PVA can visualize only the living cells *in vivo* for a long period of time, even in areas deep within large animal bodies. Copyright © 2010 John Wiley & Sons, Ltd.

Keywords: MRI; cell tracking; intracellular delivery; cell transplantation; Gd chelate

1. INTRODUCTION

Over the past decade, there has been increasing interest in developing cell transplantation therapy (1–3) for various diseases such as ischemic limbs (4), infarcted myocardium (5,6) and diabetic retinopathy (7). In particular, the transplantation of autologous cells such as bone marrow- or fat tissue-derived mesenchymal stem cells is much safer than heterologous transplantation in terms of rejection, and is promising in clinical use. However, the mechanism of cell transplantation therapy remains a matter of debate. One possible mechanism is the differentiation of transplanted cells into functional cells, and another is the paracrine effect due to the produced cytokines (8). Moreover, even the engraftment ratio and survival period of the transplanted cells remain unclear. A general method of analyzing the transplanted cells, such as immunostaining, cannot be used for autologous cell transplantation because there is no phenotypic difference between transplanted cells and host cells. In recent years, then, noninvasive tracking systems for cell transplantation are attracting a great deal of attention (9,10).

Optical imaging methods using fluorescence- or bioluminescence-labeled cells have been studied extensively (11,12). Recently, green fluorescent protein (GFP)-transgenic animal or GFP-positive cells have become widely available and have been easily analyzed using various *in vivo* optical imaging instruments. However, since optical lights can penetrate tissues less than 10 mm in the case of fluorescence and 30 mm in the case of bioluminescence, only mice or rats can be used in this system (13). Therefore, cell transplantation model systems cannot be used for various diseases in large animals (14–16). In addition, the resolution is low, and the transplanted cells can be detected as large circles in small animals (13).

In contrast, magnetic resonance imaging (MRI) is a more promising system because of its high resolution, its absence of limitations on animal size and its noninvasiveness. In order to detect the transplanted cells in host tissues using MRI, cells should be labeled with contrast agents. In the past 15 years, superparamagnetic iron oxide particles (SPIO) have been studied as a means of labeling cells because of their high sensitivity (17,18). SPIO are superior to other contrast agents in terms of the detection of cells. Rice *et al.* reported the homing phenomena of adipose-derived stem cells in cerebral infarction (19). Stuckey *et al.* reported the monitoring of bone marrow stromal cells in the infarcted heart (20). Targeted cells were usually labeled with SPIO by the endocytosis mechanism or by using gene-transfection agents. However, in long-term tracking of cells, one of the problems with this system is the fate of SPIO which leaks out of

* *Correspondence to: T. Yamaoka, Department of Biomedical Engineering, Advanced Medical Engineering Center, National Cardiovascular Center Research Institute, Suita 565-8565, Japan.*
E-mail: yamtet@ri.ncvc.go.jp

a *Y. Tachibana, A. Mahara, T. Yamaoka*
Department of Biomedical Engineering, Advanced Medical Engineering Center, National Cardiovascular Center Research Institute, Suita 565-8565, Japan

b *J.-i. Enmi, H. Iida*
Department of Investigative Radiology, Advanced Medical Engineering Center, National Cardiovascular Center Research Institute, Suita 565-8565, Japan

Contract/grant sponsor: Ministry of Health, Labour and Welfare of Japan (Health and Labour Sciences Research Grants, Research on Nanotechnical Medical).
Contract/grant sponsor: Research Grant for Cardiovascular Diseases, Ministry of Health, Labour and Welfare of Japan; contract/grant number: 18A-2.

cells (free SPIO) due to exocytosis or cell death. Additionally, SPIO that has undergone intracellular uptake is slowly digested, releasing its iron. The free SPIO remains in the body and continues to show MR contrast, creating the potential for misunderstanding (21). Amsalem *et al.* reported that the observed MRI signals after transplantation of SPIO-labeled MSCs were not attributed to transplanted cells but to cardiac macrophages which took up the released SPIO from transplanted cells (22). Li *et al.* reported that SPIO undergoing cell death was internalized by macrophages or remained in the local tissue (23).

The most important part of cell tracking is to track only the living cells. In the present study, a novel water-soluble contrast agent was designed and an effective intracellular delivery system was established. Gd–DOTA (1,4,7,10-tetraazacyclo-dodecane-*N,N′,N″,N‴*- tetraacetic acid) was conjugated to a bioinert and highly water-soluble polymeric carrier, poly(vinyl alcohol) (PVA). PVA is known to circulate for a long period of time in the blood stream *in vivo* because of its very weak interaction with the blood cells, macrophages or tissues. It was reported that the amount of PVA ingested by macrophages was much less than that of bovine serum albumin (24). The conjugates would be expected to be eliminated from the tissues without being ingested by macrophages when they are outside of the dead cells. The intracellular delivery system of the conjugates was established using an electroporation system, and the cytotoxicity, intracellular stability, body distribution and MR-imaging ability of the contrast agent were studied *in vitro* and *in vivo*.

2. RESULTS

2.1. Synthesis of Gd–PVA (*4a–d*)

Conjugates **4a–d** were synthesized in three steps using PVA with a molecular weight of 74 800 (**1**) as shown in Scheme 1. The structure of conjugates **4a–d** was confirmed by ^{1}H-NMR spectroscopy and their characteristics are summarized in Table 1. At step 1, the introduction ratios of diamine ($m/n \times 100$ in Scheme 1) were 13.2, 7.5, 3.6 and 12.9%, respectively. At step 2, DOTA-NHS-ester was completely reacted with free NH_2 groups on **2** because the peak of 2.79 ppm had disappeared. These polymers were soluble in water and DMSO and insoluble in acetone, toluene and tetrahydrofuran. The Gd (III) content of the conjugates (**4a–d**) was analyzed by inductively coupled plasma atomic emission spectroscopy. To observe the cell labeling efficiency and the intracellular distribution of the conjugates, Gd–PVA labeled with fluorescence (**4d**) was synthesized. MR imaging of labeled cells was carried out after confirming the cell uptake of **4d** with fluorescent microscopy. By contrast, the cytotoxicity assay was performed using **4b** without FITC because the wavelength of FITC overlapped with that of the WST assay.

The increase of the relaxivities (R_1) of **4a–d** with the increased introduction ratio of DOTA may be due to an increased rotational correlation and constructive restriction of motion. A maximum reflexivity value of 7.1 $mM^{-1}\,s^{-1}$ was observed at 13.2 mol% (**4a**). All of the relaxivities of **4a–d** were higher than that of clinically used Gd–DTPA (5.1 $mM^{-1}\,s^{-1}$), suggesting that each conjugate can be used as an effective contrast agent.

2.2. *In vitro* T_1-weighted MR measurements of polymer solutions

Figure 1 shows the MR images of **4d** solutions with different concentrations at 4.7 T. The T_1-weighted MRI signal of the **4d** solution increased with the increased polymer unit concentration. Significant contrast enhancement was seen over 0.2 mM. To achieve cell imaging, it is necessary to introduce the contrast agents at sufficient concentrations in the cells.

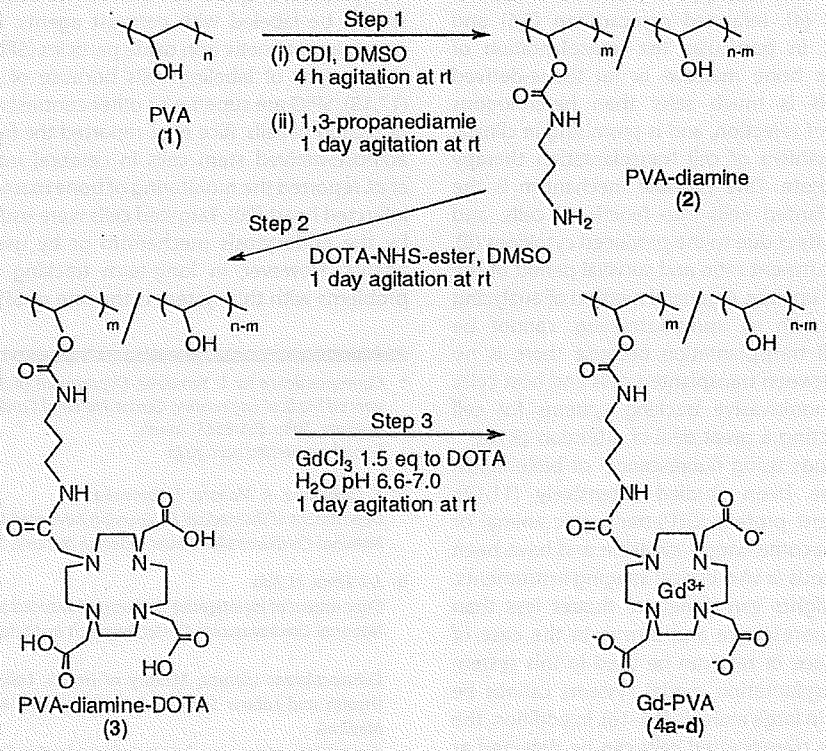

Scheme 1.

Table 1. Synthesis of **4a–d** with different contents of gadolinium chelates

	Introduction ratio of DOTA[a] (mol%)	Mn[b] (×10^5)	M_w/M_n[b]	Gd[c] (wt%)	Gd/DOTA (mol%)	FITC label	R_1 (mM^{-1} s^{-1})
4a	13.2	1.6	1.1	12.0	70.0	–	7.1
4b	7.5	1.1	1.2	9.2	69.1	–	6.2
4c	3.6	1.2	1.2	5.8	67.0	–	6.2
4d	12.9	—	—	9.3	53.9	+	7.0

[a]Scheme 1, *m/n* × 100.
[b]Determined by size exclusion chromatography using 0.25 mM phosphate buffer as eluent with polystyrene standards.
[c]Determined by inductively coupled plasma atomic emission spectroscopy measurement.

2.3. Cytotoxicity of Gd–PVA to NIH-3T3 cells and cell labeling by electroporation

Gd–PVA **4b** was used for a cytotoxicity assay since FITC introduced to **4d** obstructs the accurate WST-1 assay. The viability of NIH-3T3 cells in the presence of **4b** was not affected even at high concentrations (10 mM; polymer unit concentration in culture medium) for up to 3 days (see Supplementary Information). The low affinity of PVA (24) might suppress the interaction of Gd–PVA with the cell membrane and decrease the cytotoxicity. In fact, weak interaction was demonstrated by a simple experiment as follows. Compound **4d** was added to the culture medium of NIH-3T3 cells, and the cells were incubated for 1 h. After washing with PBS three times, no fluorescence induced by **4d** was observed, indicating that **4d** was unable to attach to the cell membrane or enter the cells spontaneously.

To deliver such a bio-inert substance into cells, we selected an electroporation method that is mainly used to transfect DNA into cells. Since this method can introduce a large amount of polymeric substances into any kind of cells nonspecifically with low cytotoxicity, it is suitable for labeling various cells including established cell lines, somatic stem cells, or even embryonic stem cells for cell transplantation (25,26). When electroporation was carried out, the concentration of Gd–PVA in culture medium was set to 10 mM (polymer unit concentration) based on the result of the cytotoxicity assay.

Figure 2 shows bright field and fluorescent photomicrographs of NIH-3T3 cells 3 days after electroporation with **4d**. Almost all cells were labeled efficiently, and the intracellular **4d** was interestingly located only in the cytosolic compartment of NIH-3T3 cells even after cell proliferation. This intracellular distribution pattern is different from that for endocytosis, which is made from bright dots.

The stability of Gd–PVA in NIH-3T3 cells was assessed by measuring the total fluorescence intensity of the growing NIH-3T3 cells with time. The number of Gd(III) molecules in one cell calculated from the fluorescence intensity was 7.3 × 10^8 per cell just after electroporation. Cells were cultured for a given period of time without subculture and then lysed. Before the cells were lysed, they were washed by PBS sufficiently to eliminate any **4d** leaching from them. Figure 3 represents the total fluorescence intensity of **4d** in NIH-3T3 cells (solid circle) and cellular proliferation rates (open circle). Fluorescence derived from **4d** in cells showed no significant change over 10 days, and the labeled cells grew well. These results show that **4d** can remain in the cytosolic compartment stably for a long period of time without having any effect on cell proliferation.

2.4. *In vitro* T_1-weighted MR measurements of the labeled NIH-3T3

Figure 4a shows an MR image of the NIH-3T3 cell suspensions at 4.7 T. Compound **4d**-labeled NIH-3T3 cell suspension, non-labeled NIH-3T3 cell suspension and cell-free and Gd-free medium were left at rest for 1 day to allow the cells to be precipitated to the bottom of the test tube. Clear signal enhancement in tube 1 at slice B passing through the precipitated cells was seen. On the other hand, no signal was observed in tube 1 at slice A, which indicates that **4d** did not leak out of the cells and that **4d** in cells gives sufficient MR contrast irrespective of the small amount of free water in the cells

To examine the cell density dependence of signal enhancement, we next acquired MR images of **4d**-labeled NIH-3T3 cells at different densities in agarose gel, which was used to fix the transplanted cells in the experiment involving the injection of cells into a rat (Fig. 4b). MRI can depict at least 3.5 × 10^6 NIH-3T3 cells. The number of cells transplanted to the rat ischemic hind limb model (27) or infarcted myocardium swine model (28) was 1 × 10^7 or 5 × 10^7, respectively. The sensitivity shown in Fig. 4 revealed that our imaging agent would surely be useful for

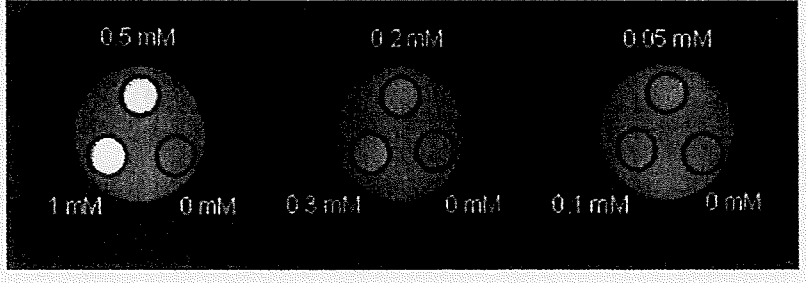

Figure 1. XXX[Q1]

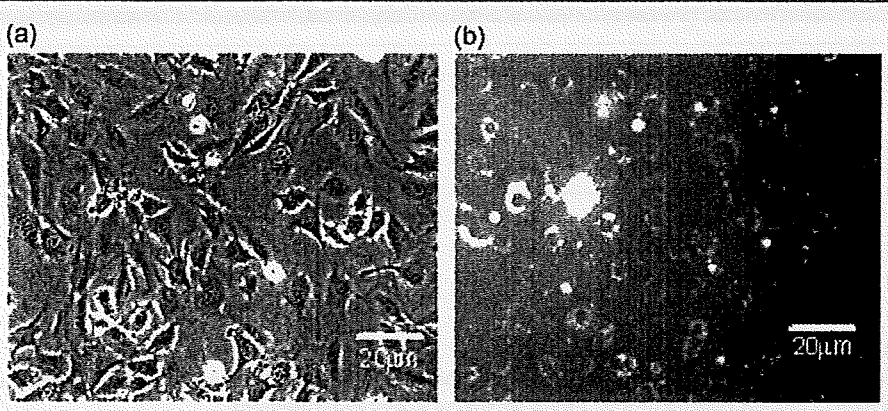

Figure 2.

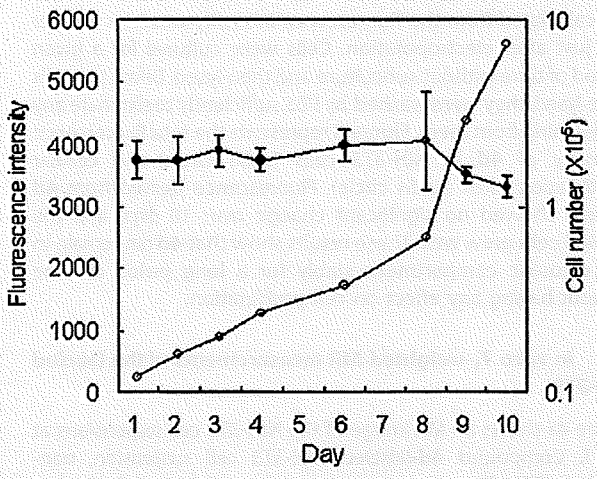

Figure 3.

tracking this range of transplanted cells *in vivo*. Future studies should focus on high labeling efficiency at higher concentrations of **4d** using electroporation or another method.

2.5. *In vivo* fate of free SPIO and free Gd–PVA

To detect the living cells, contrast agents present outside of the labeled cells (free contrast agent) after cell death should be eliminated from the transplantation site. Solutions of **4d** and SPIO injected into the tissue were used as the model for free contrast agents. Solutions of **4d** and SPIO were directly injected into rat femoral muscles, and on days 0, 3 and 6, the MR image was analyzed (Fig. 5). Representative slices are shown in Fig. 5. The bright signal attributed to **4d** weakened rapidly and was observed only slightly on day 3. In contrast, the dark signal due to SPIO remained in the same area and was clearly observed even 10 days after the injection. The same tendency was observed in the other slices. SPIO-derived contrast several days after injection may be attributed to the phagocytes engulfing the injected SPIO, as has been previously reported (22,23). Furthermore, the time courses of the contrast-to-noise ratio (CNR) and the volume of the contrast-enhanced region were evaluated (Fig. 6). For SPIO, the CNR and the volume of the contrast-enhanced region showed no significant decrease over the course of 13 days. In contrast, these same parameters decreased rapidly when **4d** was used. Signal enhancement was observed in only one out of three rats at 4 days after injection. Therefore, the data of **4d** at 4 days have no error bar. Signal enhancement due to **4d** disappeared completely in all rats at 6 days after injection. These data showed the rapid clearance of Gd–PVA from muscle and the long-term retention of SPIO in muscle. Yamaoka *et al.* reported that the half-life period of radio-labeled PVA (molecular weight of 74 800) after i.m. injection was about 10 h (38). As shown in Fig. 6, the half-life period of free Gd–PVA from the tissue was about 10 hs, which was almost the same as that of PVA. This result suggested that free Gd–PVA behaved like free PVA without interacting

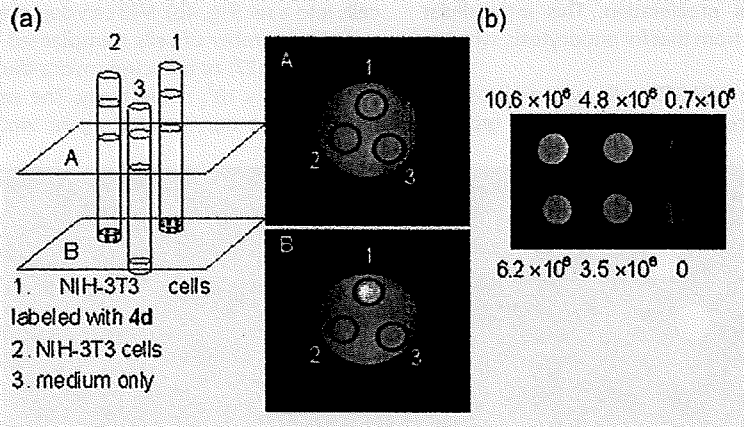

Figure 4.

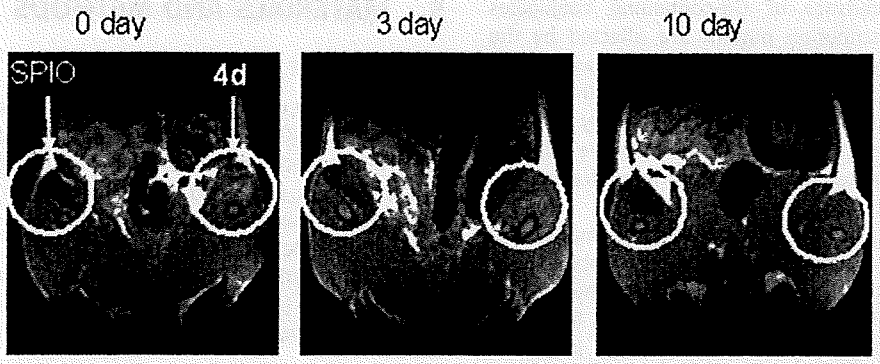

Figure 5.

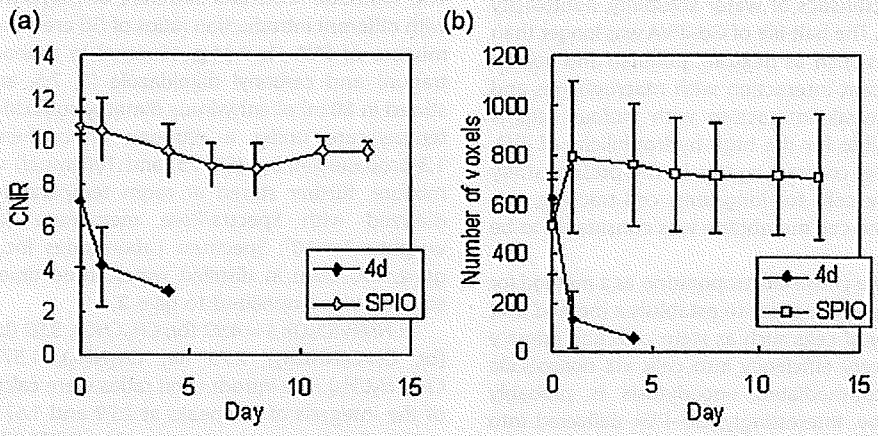

Figure 6.

with macrophages *in vivo*. It can then be considered that the MR contrast of Gd–PVA is attributable to the living cells *in vivo*.

2.6. Preliminary *in vivo* MR imaging of transplanted NIH-3T3 cells

Figure 7 shows an MR image of a rat that received subcutaneous transplantation of 2×10^7 **4d**-labeled NIH-3T3 cells entrapped in agarose gel and cell-free gel (control) at each side of the back. In this preliminary MR imaging, we used undegradable agarose gel to evaluate the MRI contrast at a known density of cells. Strong contrast enhancement was observed at the area where labeled NIH-3T3 cells were transplanted, while the control gel revealed a dark shadow.

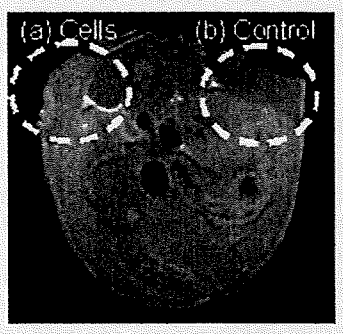

Figure 7.

These results indicate that transplanted cells can be detected *in vivo* at a cell density of 10^7 cells per 0.1 ml.

3. DISCUSSION

Our goal was to track only the living cells *in vivo* for a long period of time. To this end, an MRI contrast agent with adequate characteristics for cell labeling and delivery system into the cells is a key factor. Cell labeling using SPIO as a contrast agent was reported in detail by Engberink *et al.* in 2007 (29). They cocultured human monocytes with SPIO suspension at a concentration of 1.0 mg Fe ml^{-1} for 0–6 h. Incubation with SPIO resulted in effective cell labeling by endocytosis, nonspecifically. The detection limit was 0.5×10^6 labeled cells per 250 µl on a 4.7 T MRI scanner. SPIO permits the detection of a small number of cells because of its high sensitivity. In general, however, endocytosed substrates would be exocytosed over time. The MR contrast obtained after SPIO-labeled cell transplantation was not attributed to the transplanted cells but to the macrophages that engulfed the free SPIO (22,23). In this study, MR imaging data for SPIO solution in femoral muscle showed that, even at 10 days after injection, SPIO still remained. These data suggested that SPIO is less suitable for long-term cell tracking. To track the transplanted cells for a long period of time, the labeling agent released upon cell death should be eliminated from the tissue.

Since we found that low-molecular-weight Gd-chelates cannot remain in cells stably (data not shown), water-soluble conjugates of Gd-chelates and a bio inert water-soluble carrier were

designed. The characteristics of Gd-containing conjugates including the body distribution pattern are affected by the nature of the carrier polymer. The water-soluble contrast agent is expected to be eliminated from the body once it exits the cells if a truly bio-inert carrier molecule is selected. To track only the living cells, the contrast agents should be designed to be different from the conventional water-soluble imaging agent for vascular inflammation imaging or vascular imaging (30–36).

We selected PVA in this experiment as the carrier material for long-term living cell tracking. Selecting nondegradable PVA as the carrier enabled us to evaluate the potential of the contrast agent in intracellular distribution or in cell tracking for a long period of time. The body distribution of various polymeric carriers has been extensively studied (37,38). Among these carriers, PVA has various advantages as a candidate for use in the biomedical and pharmaceutical fields. Some of these advantages include its characteristics of water solubility, nontoxicity and noncarcinogenicity. The half-life of Gd–PVA was longer than those of other polymers such as dextran, pullulan and gelatin because of an insignificant interaction with macrophages and blood cells (24). This weak interaction with various cells is believed to be responsible for the high hydrophilicity of PVA. Since we proposed novel contrast agents in the present study that would not exit the cells for long-term cell tracking, this weak interaction with the cell membrane was considered to be an advantage.

In the present study, we chose electroporation as a method for delivering Gd–PVA into cells in order to establish a method that is applicable to a variety of cells such as stem cells and primary cells. The material delivery efficiency into cells via nonspecific endocytosis or receptor-mediated encodytosis is probably affected by the cell type. Interestingly, Gd–PVA delivered into cells was localized only in the cytosolic compartment even after cell proliferation (Fig. 2), although the reason for this remains unclear.

One possible issue in living cell tracking, although unlikely to occur, is the uptake of dying cells labeled with **4d** by tissue macrophages that remain in the tissue. To study this possibility, it is necessary to perform an experiment using cells in different states (viable, dying and dead). However, it is difficult to control the states of transplanted cells. We are considering evaluating the effect of macrophages on the fate of Gd–PVA by transplanting irradiated cells with sublethal doses or by xenografting Gd–PVA-labeled cells.

Long-term cell tracking will be feasible due to the high stability of Gd–PVA in cells for a long period of time (Fig. 3). In contrast to SPIO, the free Gd–PVA will be eliminated from the tissue (Fig. 5) when the transplanted cells burst upon cell death. The imaging of only the living cells might be achieved using Gd–PVA.

4. CONCLUSION

The novel MRI contrast agents composed of PVA and Gd showed high relaxivity and low cytotoxicity. The growing rate of NIH-3T3 cells was not affected by the intracellularly delivered Gd–PVA. Furthermore, Gd–PVA was retained stably in cells for at least 10 days. The *in vitro* T_1-weighted MR measurements using NIH-3T3 cells revealed that cells could be visualized under MRI. This *in vivo* study demonstrates for the first time that Gd–PVA has high applicability as a novel contrast agent for tracking only living cells.

5. MATERIALS AND METHODS

5.1. Materials

PVA (M_w: 74,800, degree of saponification 98%) was a kind gift from Kuraray Co. Ltd (Okayama, Japan). 1,4,7,10-Tetraazacyclododecane-1,4,7,10-tetraacetic acid mono(*N*-hydroxysuccinimidyl ester) (DOTA-NHS-ester) was purchased from Macrocyclics (Dallas, TX, USA). FITC-NHS-ester was purchased from Invitrogen (Eugene, OR, USA). Gadolinium chloride ($GdCl_3$) was purchased from Wako Pure Chemical Industries (Osaka, Japan). Resovist was purchased from Nihon Schering (Osaka, Japan). Other reagents and solvents were commercially available and used as received.

5.2. Synthesis of Gd–PVA

The synthetic route and structure of polymeric contrast agents with different introduction ratios of Gd are shown in Scheme 1. A mixture of PVA (**1**; 0.44 g, 10 mmol in monomer unit concentration) and carbonyl diimidazole (5, 7.5, and 10 mmol) was stirred in 80 ml of anhydrous dimethylsulfoxide (DMSO) at room temperature under a nitrogen atmosphere for 4 h. Then, 1,3-propanediamine (50, 75, and 100 mmol) was added to the mixture, further stirred at room temperature for 1 day, and dialyzed with Spectra/Pore membrane (cut-off molecular weight = 1×10^4; Spectrum Laboratories Inc., Rancho Dominguez, CA, USA) in distilled water three times. The remaining solution was lyophilized to give **2**.

^{1}H NMR (D_2O): δ = 4.92 (br, CH_2CHO), 3.92 (br, CH_2CHOH), 3.10 [br, $C(=O)NHCH_2$], 2.79 (br, CH_2NH_2), 1.57 (br, $CHCH_2$, br, $CH_2CH_2CH_2$). The introduction ratios were calculated as the ratio of the integrals of the peaks at 2.79 and 1.57 ppm.

PVA-diamine was reacted with DOTA-NHS-ester (NH_2 of FITC-PVA-diamine: DOTA-NHS-ester = 1:1.5) in 80 ml of anhydrous DMSO at room temperature for 1 day under a nitrogen atmosphere. The reaction mixture was dialyzed in distilled water three times, and lyophilized to give PVA-diamine-DOTA (**3**).

^{1}H NMR (D_2O): δ = 5.07 (br, CH_2CHO), 4.06 (br, CH_2CHOH), 3.86 [br, $C(=O)CH_2N$)] 3.51 [br, $NCH_2C(=O)OH$], 3.24 [br, $C(=O)NHCH_2$, br, CH_2CH_2N], 1.69 (br, $CHCH_2$, br, $CH_2CH_2CH_2$).

The solution of **3** was then treated with the dropwise addition of 1.5 mole equiv. of gadolinium chloride to the DOTA while stirring. The pH was maintained between 6.6 and 7.0 with 1 M NaOH solution and stirred for an additional 24 h at room temperature. The reaction mixture was dialyzed in distilled water three times and lyophilized to give Gd–PVA (**4a–d**).

For labeling Gd–PVA with FITC, PVA–diamine was mixed with a small amount of FITC–NHS–ester (NH_2 of **2**: FITC–NHS–ester = 1: 8×10^{-5}) and stirred in 80 ml of anhydrous DMSO at room temperature for 1 day under a nitrogen atmosphere. The reaction mixture was dialyzed, lyophilized to give FITC-PVA-diamine and subjected to the DOTA reaction as shown in Scheme 1.

5.3. Measurements

^{1}H-NMR spectra were recorded on a 300 MHz NMR spectrometer (Gemini2000/300; Varian Inc., CA, USA) with a sample concentration of 8 mg per 800 µl. Size exclusion chromatography analysis was carried out using Shimadzu Gel Permeation Chromatography System apparatus equipped with a refractive index and UV detectors under the following conditions: TSKgel G6000PWXL and G3000PWXL columns and 0.067 M PBS eluent at

a flow rate of 0.3 ml min^{-1} at 40°C (Tosoh, Tokyo, Japan) with a sample concentration of 1 mg per 100 μl. The concentration of the paramagnetic species [Gd(III)] was measured by inductively coupled plasma atomic emission spectroscopy (model 7510, Shimadzu Co., Kyoto, Japan).

5.4. Relaxivity of conjugated Gd at 7.1 T

Solvent longitudinal relaxation times (T_1) in the aqueous solutions of the gadolinium conjugate were measured at different concentrations of gadolinium conjugate using a mixture of distilled water (0.625%) and deuterium oxide (99.375%) as a solvent. All measurements were performed on a 300 MHz (7.1 T) NMR spectrometer (Gemini2000/300; Varian Inc., CA, USA) using an inversion recovery technique with 19 inversion times (*TI*) ranging from 1 to 5000 ms at ambient temperature (25°C) with a sample concentration of 8 mg per 800 μl. A typical pulse width of 180° pulse was 19 μs. T_1 values were estimated using least-squares fitting of the signal intensities measured at 19 *TI* values in an exponential fashion. The relaxivity of each gadolinium complex was determined by a linear regression of the $1/T_1$ vs the gadolinium complex concentration.

5.5. Cell culture

NIH-3T3 cells were used for evaluating the cytotoxicity, cell labeling potential and imaging efficiency of the Gd–PVA. They were grown in Dulbecco's modified Eagle's medium (DMEM-LG) supplemented with 10% bovine calf serum, 100 units ml^{-1} penicillin, and 100 units ml^{-1} streptomycin at 37°C, 10% CO_2 atmosphere.

5.6. Cytotoxicity assay

NIH-3T3 cells (1×10^4 cells per well) were seeded in a 96-well culture plate and cultured overnight. Varying concentrations (polymer unit concentrations of 10 nM to 10 mM) of **4b** were added to each well. At the indicated time points, the number of cells was measured by WST-1 assay according to the manufacturer's protocol (Takara Shuzo, Otsu, Japan). Briefly, cells were washed with PBS three times, and the culture medium (100 μl) was added to each well. Ten microliters of WST-1 {4-[3-(4-iodophenyl)-2-(4-nitrophenyl)-2H-5-tetrazolio]-1,3-benzene disulfonate} solution was added to each well, and the plates were incubated for 30 min. The absorbance at 450 nm was measured on a microplate reader (Model 550, Bio-Rad Laboratory Co., Tokyo, Japan).

5.7. Cell labeling by electroporation

NIH-3T3 cells were cultured in a 6 cm diameter Petri dish at a concentration of 5×10^5 cells per dish in DMEM-LG for 1 day. An arbitrary amount of **4d** was added to the culture medium, and electrical pulses were applied to cells using a CUY-21 electroporator (CUY-21; NEPPA GENE, Tokyo, Japan). Rectangular electrical pulses (field strength 300 V cm^{-1}, number of pulses 10, pulse duration 5 ms) were applied to cells using two parallel electrodes with a 5 mm gap. Cells were incubated for 1 h and washed with PBS twice.

5.8. Stability of 4d in cells

To determine whether **4d** molecules stay in NIH-3T3 cells for a long period of time, the labeled cells (1×10^4 cells) were seeded in a 6 cm diameter Petri dish and cultured over 10 days without a subculture. The time course of the fluorescence intensity for the cultured cells was measured as follows. Before each measurement, cells in one dish were washed three times with PBS to eliminate the free **4d** from the cells and lysed in 1 ml lysis buffer [25 mM tris (pH 7.8), 2 mM dithiothreitol, 2 mM 1,2-diaminocyclohexan-*N*,*N*,*N*′,*N*′-tetraacetic acid, 10% glycerol, 1% Triton X-100]. After 1 h incubation at 37°C, the fluorescence intensity of the cell lysates was measured with a spectrofluorometer (excitation 430 nm, emission 540 nm, Wallac 1420 ARVOsx, Perkin-Elmer Life Sciences, Boston, MA, USA). The time course of the fluorescence intensity represented the stability of **4d** in the cells. At the same time, the number of cells in each dish was counted. In addition, the amount of **4d** delivered into each cell by electroporation was calculated using the standard curve of fluorescence intensity.

5.9. MR imaging of Gd–PVA solution at 4.7 T

MR images of **4d** aqueous solutions were obtained on a 200-MHz (4.7 T) NMR spectrometer (Apollo; Tecmag Inc., TX, USA) equipped with a gradient system (Jeol Ltd, Tokyo, Japan; maximum gradient strength 20 mT m^{-1}; slew late 50 mT m^{-1} ms^{-1}) using a saddle coil with an inner diameter of 47 mm. Aqueous solutions with different concentrations (0.05, 0.1, 0.2, 0.3, 0.5 and 1 mM) of polymer unit were prepared. Three test tubes with different concentrations were fixed vertically. A horizontal section was scanned. T_1-weighted images of the samples were acquired using a 2D spin echo sequence with a repetition time (*TR*) of 2000 ms and an echo time (*TE*) of 16 ms. Taking the long T_1 of the water observed in the 1.5 T machine into account, *TR* was greater in comparison to that for general T_1-weighted images. We used the minimum possible *TE* to minimize the T_2 relaxation effect. Other scanning parameters were as follows: field of view (FOV), 6 × 6 cm; matrix, 256 × 256; slice thickness, 1 cm.

5.10. MR imaging of NIH-3T3 cells *in vitro*

MR measurements of labeled cells were performed using the same scanner and the same parameters as in the imaging of **4d** solutions. Cells labeled with **4d** by electroporation were trypsinized, centrifuged and resuspended in test tubes (75 mm long, 10 mm in diameter) at 7×10^6 cells in 2 ml of complete DMEM. The test tubes with labeled cell suspensions were allowed to settle for 1 day to allow the cells to be precipitated before MR imaging. A test tube with unlabeled cell suspensions was also prepared in the same manner. In addition, a test tube with cell-free pure medium was prepared. The three test tubes prepared were arranged as shown in Fig. 4(a). Scanned slices were positioned so that they pass through the cell pellet part (slice B in Fig. 4a) or the solution part (slice A in Fig. 4a).

The cell density dependence of signal enhancement was examined as follows. Different numbers of labeled cells were suspended in 100 μl of agarose solution at the concentration of 2 wt% and cooled to be gelated. The MR imaging data of these mixtures were collected by a 1 T compact MR imaging system with a permanent magnet (MRmini, Dainippon Sumitomo Pharma, Osaka, Japan) with a *TE* of 9 ms and a *TR* of 1500 ms (FOV, 3 × 6 cm; matrix, 128 × 256; slice thickness, 3.7 mm).

5.11. *In vivo* fate of free SPIO and free Gd–PVA

The clearance of **4d** and SPIO after intramuscular injection was investigated in male rat F344. The rat was anesthetized by inhalation anesthesia (1.5% isoflurane). Solutions of **4d** (Gd

0.8 μmol per 50 μl water) and carboxydextran-coated SPIO, Resovist™ (Fe 0.8 μmol per 50 μl water, Bayer, Osaka, Japan) were injected into the left and right femoral muscles, respectively, using a 29 G needle. Whole inferior limbs of the animal were scanned at 0, 3 and 10 days after injection on a 1.5 T compact MR imaging system. These images were obtained with a *TR* of 1500 ms and a *TE* of 9 ms (FOV, 4 × 8 cm; matrix, 128 × 256; slice thickness, 1 mm; slice gap, 0 mm; number of slice, 35).

For the time course of the CNR and the number of voxels in the region, whole inferior limbs of the animal were scanned at 0, 1, 4, 6, 8, 11 and 13 days after injection on a 1.5 T compact MR imaging system. These images were obtained with a *TR* of 500 ms and a *TE* of 9 ms, and with a *TR* of 3000 ms and a *TE* of 20 ms (FOV, 4 × 8 cm; matrix, 128 × 256; slice thickness, 1 mm; slice gap, 0 mm; number of slices, 35). CNR was calculated as $(\pi/2)^{1/2}|S_1-S_2|/S_{air}$, where S_1, S_2 and S_{air} were the mean intensities in the contrast-enhanced region, muscle and air, respectively.

5.12. Preliminary MR imaging of transplanted NIH-3T3 cells

In vivo cell tracking was preliminarily performed in male Balb/c mice. These mice were anesthetized for imaging with the use of a general inhalation anesthesia (1.5% isoflurane) and were allowed to breathe spontaneously during preparation and scanning. NIH-3T3 cells labeled with **4d** (2×10^7 cells) were embedded in 2 wt% agarose gel (200 μl) and transplanted to the mice subcutaneously. MR images were obtained using a 2 T compact MR imaging system with a permanent magnet. T_1-weighted images were acquired using a 2D spin echo sequence with a *TR* of 2000 ms and a *TE* of 9 ms (FOV, 3 × 6 cm; matrix, 128 × 256; slice thickness, 1 mm) at room temperature.

6. SUPPORTING INFORMATION

Supporting information can be found in the online version of this article.

Acknowledgements

This work was supported by grants-in-aid from the Ministry of Health, Labour and Welfare of Japan (Health and Labour Sciences Research Grants, Research on Nanotechnical Medical). This work was also supported by a Research Grant for Cardiovascular Diseases (18A-2) from the Ministry of Health, Labour and Welfare of Japan.

References

1. Perin EC, Dohmann HF, Borojevic R, Silva SA, Sousa AL, Mesquita CT, Rossi MI, Carvalho AC, Dutra HS, Dohmann HJ, Silva GV, Belem L, Vivacqua R, Rangel FO, Esporcatte R, Geng YJ, Vaughn WK, Assad JA, Mesquita ET, Willerson JT., Transendocardial, autologous bone marrow cell transplantation for severe, chronic ischemic heart failure. Circulation 2003; 107 18 2294–2302.
2. Schmid C, Schleuning M, Schwerdtfeger R, Hertenstein B, Mischak-Weissinger E, Bunjes D, Harsdorf SV, Scheid C, Holtick U, Greinix H, Keil F, Schneider B, Sandherr M, Bug G, Tischer J, Ledderose G, Hallek M, Hiddemann W, Kolb HJ. Long-term survival in refractory acute myeloid leukemia after sequential treatment with chemotherapy and reduced-intensity conditioning for allogeneic stem cell transplantation. Blood 2006; 108(3): 1092–1099.
3. Slavin S, Nagler A, Naparstek E, Kapelushnik Y, Aker M, Cividalli G, Varadi G, Kirschbaum M, Ackerstein A, Samuel S, Amar A, Brautbar C, Ben-Tal O, Eldor A, Or R. Nonmyeloablative stem cell transplantation and cell therapy as an alternative to conventional bone marrow transplantation with lethal cytoreduction for the treatment of malignant and nonmalignant hematologic diseases. Blood 1998; 91(3): 756–763.
4. Kim SW, Han H, Chae GT, Lee SH, Bo S, Yoon JH, Lee YS, Lee KS, Park HK, Kang KS. Successful stem cell therapy using umbilical cord blood-derived multipotent stem cells for Buerger's disease and ischemic limb disease animal model. Stem Cells 2006; 24(6): 1620–1626.
5. Stamm C, Westphal B, Kleine HD, Petzsch M, Kittner C, Klinge H, Schumichen C, Nienaber CA, Freund M, Steinhoff G. Autologous bone-marrow stem-cell transplantation for myocardial regeneration. Lancet 2003; 361(9351): 45–46.
6. Strauer BE, Brehm M, Zeus T, Kostering M, Hernandez A, Sorg RV, Kogler G, Wernet P. Repair of infarcted myocardium by autologous intracoronary mononuclear bone marrow cell transplantation in humans. Circulation 2002; 106(15): 1913–1918 .
7. Grant MB, May WS, Caballero S, Brown GA, Guthrie SM, Mames RN, Byrne BJ, Vaught T, Spoerri PE, Peck AB, Scott EW. Adult hematopoietic stem cells provide functional hemangioblast activity during retinal neovascularization. Nat Med 2002; 8(6): 607–612.
8. Tang YL, Zhao Q, Qin X, Shen L, Cheng L, Ge J, Phillips MI. Paracrine action enhances the effects of autologous mesenchymal stem cell transplantation on vascular regeneration in rat model of myocardial infarction. Ann Thorac Surg 2005; 80(1): 229–236 discussion 236-227.
9. Beeres SL, Bengel FM, Bartunek J, Atsma DE, Hill JM, Vanderheyden M, Penicka M, Schalij MJ, Wijns W, Bax JJ. Role of imaging in cardiac stem cell therapy. J Am Coll Cardiol 2007; 49(11): 1137–1148.
10. Frangioni JV, Hajjar RJ. In vivo tracking of stem cells for clinical trials in cardiovascular disease. Circulation 2004; 110(21): 3378–3383.
11. Tanaka M, Swijnenburg RJ, Gunawan F, Cao YA, Yang Y, Caffarelli AD, de Bruin JL, Contag CH, Robbins RC. In vivo visualization of cardiac allograft rejection and trafficking passenger leukocytes using bioluminescence imaging. Circulation 2005; 112(9 Suppl): I105–110.
12. Wang X, Rosol M, Ge S, Peterson D, McNamara G, Pollack H, Kohn DB, Nelson MD, Crooks GM. Dynamic tracking of human hematopoietic stem cell engraftment using in vivo bioluminescence imaging. Blood 2003; 102(10): 3478–3482.
13. Sutton EJ, Henning TD, Pichler BJ, Bremer C, Daldrup-Link HE. Cell tracking with optical imaging. Eur Radiol 2008; 18(10): 2021–2032.
14. Takagi Y, Takahashi J, Saiki H, Morizane A, Hayashi T, Kishi Y, Fukuda H, Okamoto Y, Koyanagi M, Ideguchi M, Hayashi H, Imazato T, Kawasaki H, Suemori H, Omachi S, Iida H, Itoh N, Nakatsuji N, Sasai Y, Hashimoto N. Dopaminergic neurons generated from monkey embryonic stem cells function in a Parkinson primate model. J Clin Invest 2005; 115(1): 102–109.
15. Takahashi M, Nakamura T, Toba T, Kajiwara N, Kato H, Shimizu Y. Transplantation of endothelial progenitor cells into the lung to alleviate pulmonary hypertension in dogs. Tissue Eng 2004; 10(5–6): 771–779.
16. Tomita S, Mickle DA, Weisel RD, Jia ZQ, Tumiati LC, Allidina Y, Liu P, Li RK. Improved heart function with myogenesis and angiogenesis after autologous porcine bone marrow stromal cell transplantation. J Thorac Cardiovasc Surg 2002; 123(6): 1132–1140.
17. Kraitchman DL, Tatsumi M, Gilson WD, Ishimori T, Kedziorek D, Walczak P, Segars WP, Chen HH, Fritzges D, Izbudak I, Young RG, Marcelino M, Pittenger MF, Solaiyappan M, Boston RC, Tsui BM, Wahl RL, Bulte JW. Dynamic imaging of allogeneic mesenchymal stem cells trafficking to myocardial infarction. Circulation 2005; 112(10): 1451–1461.
18. Hill JM, Dick AJ, Raman VK, Thompson RB, Yu ZX, Hinds KA, Pessanha BS, Guttman MA, Varney TR, Martin BJ, Dunbar CE, McVeigh ER, Lederman RJ. Serial cardiac magnetic resonance imaging of injected mesenchymal stem cells. Circulation 2003; 108(8): 1009–1014.

19. Rice HE, Hsu EW, Sheng H, Evenson DA, Freemerman AJ, Safford KM, Provenzale JM, Warner DS, Johnson GA. Superparamagnetic iron oxide labeling and transplantation of adipose-derived stem cells in middle cerebral artery occlusion-injured mice. AJR Am J Roentgenol 2007; 188(4): 1101–1108.
20. Stuckey DJ, Carr CA, Martin-Rendon E, Tyler DJ, Willmott C, Cassidy PJ, Hale SJ, Schneider JE, Tatton L, Harding SE, Radda GK, Watt S, Clarke K. Iron particles for noninvasive monitoring of bone marrow stromal cell engraftment into, and isolation of viable engrafted donor cells from, the heart. Stem Cells 2006; 24(8): 1968–1975.
21. Hoshino K, Ly HQ, Frangioni JV, Hajjar RJ. In vivo tracking in cardiac stem cell-based therapy. Prog Cardiovasc Dis 2007; 49(6): 414–420.
22. Amsalem Y, Mardor Y, Feinberg MS, Landa N, Miller L, Daniels D, Ocherashvilli A, Holbova R, Yosef O, Barbash IM, Leor J. Iron-oxide labeling and outcome of transplanted mesenchymal stem cells in the infarcted myocardium. Circulation 2007; 116(11 Suppl): I38–45.
23. Li Z, Suzuki Y, Huang M, Cao F, Xie X, Connolly AJ, Yang PC, Wu JC. Comparison of reporter gene and iron particle labeling for tracking fate of human embryonic stem cells and differentiated endothelial cells in living subjects. Stem Cells 2008; 26(4): 864–873.
24. Yamaoka T, Tabata Y, Ikada Y. Comparison of body distribution of poly(vinyl alcohol) with other water-soluble polymers after intravenous administration. J Pharm Pharmacol 1995; 47(6): 479–486.
25. Walczak P, Kedziorek DA, Gilad AA, Lin S, Bulte JW. Instant MR labeling of stem cells using magnetoelectroporation. Magn Reson Med 2005; 54(4): 769–774.
26. Pillai O, Panchagnula R. Polymers in drug delivery. Curr Opin Chem Biol 2001; 5(4): 447–451.
27. Li TS, Hamano K, Suzuki K, Ito H, Zempo N, Matsuzaki M. Improved angiogenic potency by implantation of ex vivo hypoxia prestimulated bone marrow cells in rats. Am J Physiol Heart Circ Physiol 2002; 283(2): H468–473.
28. Zhang S, Ge J, Zhao L, Qian J, Huang Z, Shen L, Sun A, Wang K, Zou Y. Host vascular niche contributes to myocardial repair induced by intracoronary transplantation of bone marrow CD34+ progenitor cells in infarcted swine heart. Stem Cells 2007; 25(5): 1195–1203.
29. Oude Engberink RD, van der Pol SM, Dopp EA, de Vries HE, Blezer EL. Comparison of SPIO and USPIO for in vitro labeling of human monocytes: MR detection and cell function. Radiology 2007; 243(2): 467–474.
30. Aime S, Cabella C, Colombatto S, Geninatti Crich S, Gianolio E, Maggioni F. Insights into the use of paramagnetic Gd(III) complexes in MR-molecular imaging investigations. J Magn Reson Imag 2002; 16(4): 394–406.
31. Gustafsson B, Youens S, Louie AY. Development of contrast agents targeted to macrophage scavenger receptors for MRI of vascular inflammation. Bioconjug Chem 2006; 17(2): 538–547.
32. Langereis S, de Lussanet QG, van Genderen MH, Meijer EW, Beets-Tan RG, Griffioen AW, van Engelshoven JM, Backes WH. Evaluation of Gd(III)DTPA-terminated poly(propylene imine) dendrimers as contrast agents for MR imaging. NMR Biomed 2006; 19(1): 133–141.
33. Lu ZR, Wang X, Parker DL, Goodrich KC, Buswell HR. Poly(-l-glutamic acid) Gd(III)–DOTA conjugate with a degradable spacer for magnetic resonance imaging. Bioconjug Chem 2003; 14(4): 715–719.
34. Nakamura E, Makino K, Okano T, Yamamoto T, Yokoyama M. A polymeric micelle MRI contrast agent with changeable relaxivity. J Control Release 2006; 114(3): 325–333.
35. Wen X, Jackson EF, Price RE, Kim EE, Wu Q, Wallace S, Charnsangavej C, Gelovani JG, Li C. Synthesis and characterization of poly(L-glutamic acid) gadolinium chelate: a new biodegradable MRI contrast agent. Bioconjug Chem 2004; 15(6): 1408–1415.
36. Yan GP, Liu ML, Li LY. Polyaspartamide gadolinium complexes containing sulfadiazine groups as potential macromolecular MRI contrast agents. Bioconjug Chem 2005; 16(4): 967–971.
37. Yamaoka T, Tabata Y, Ikada Y. Distribution and tissue uptake of poly(ethylene glycol) with different molecular weights after intravenous administration to mice. J Pharm Sci 1994; 83(4): 601–606.
38. Yamaoka T, Tabata Y, Ikada Y. Fate of water-soluble polymers administered via different routes. J Pharm Sci 1995; 84(3): 349–354.

Bioorganic & Medicinal Chemistry 18 (2010) 3946–3950

Contents lists available at ScienceDirect

Bioorganic & Medicinal Chemistry

journal homepage: www.elsevier.com/locate/bmc

Liver-targeted siRNA delivery by polyethylenimine (PEI)-pullulan carrier

Jeong-Hun Kang [a,†], Yoichi Tachibana [b,†], Wakako Kamata [b,†], Atsushi Mahara [b], Mariko Harada-Shiba [c], Tetsuji Yamaoka [b,d,*]

[a] Laboratory for Advanced Diagnostic Medical Devices and Department of Biomedical Engineering, Advanced Medical Engineering Center, National Cardiovascular Center Research Institute, 5-7-1 Fujishiro-dai, Suita, Osaka 565-8565, Japan
[b] Department of Biomedical Engineering, Advanced Medical Engineering Center, National Cardiovascular Center Research Institute, 5-7-1 Fujishiro-dai, Suita, Osaka 565-8565, Japan
[c] Department of Bioscience, Advanced Medical Engineering Center, National Cardiovascular Center Research Institute, 5-7-1 Fujishiro-dai, Suita, Osaka 565-8565, Japan
[d] CREST, Japan Science and Technology Corporation, 5 Sanbancho, Chiyoda-ku, Tokyo 102-0075, Japan

ARTICLE INFO

Article history:
Received 5 March 2010
Revised 12 April 2010
Accepted 13 April 2010
Available online 18 April 2010

Keywords:
Polyethylenimine
Gene delivery
Cationic polymer
Cytotoxicity

ABSTRACT

Recently, small interfering RNA (siRNA)-based therapeutics have been used to treat diseases. Efficient and stable siRNA delivery into disease cells is important in the use of this agent for treatment. In the present study, pullulan was introduced into polyethylenimine (PEI) for liver targeting. PEI/siRNA or pullulan-containing PEI/siRNA complexes were delivered into mice through the tail vein either by a hydrodynamics- or non-hydrodynamics-based injection. The incidence of mortality was found to increase with an increase in the nitrogen/phosphorus (N/P) ratio of PEI/siRNA complexes. Moreover, the hydrodynamics-based injection increased mice mortality. Introduction of pullulan into PEI dramatically reduced mouse death after systemic injection. After systemic injection, the PEI/fluorescein-labeled siRNA complex increased the level of fluorescence in the lung and the PEI-pullulan/siRNA complex led to an increased fluorescence level in the liver. These results suggest that the PEI-pullulan polymer may be a useful, low toxic means for efficient delivery of siRNA into the liver.

1. Introduction

Small interfering RNA (siRNA)-based therapeutics, which are now recognized as a medical approach for the treatment of difficult-to-cure diseases such as viral infections and tumors, are attracting considerable attention in recent times.[1,2] However, naked siRNA is unstable in the bloodstream and is rapidly eliminated through the urinary system. Moreover, its negative charge inhibits efficient cellular uptake due to the negative charge of the cell surface. Thus, efficient and stable siRNA delivery into diseased cells is critical in this treatment modality. Many researchers have attempted to induce various chemical modifications into siRNA or to form complexes with several cationic carriers such as cationic polymers, liposomes, peptides, or proteins.[3–5]

Among cationic polymers, polyethylenimine (PEI) is the most popular synthetic polymer and has a high cationic charge density. It has been widely used to deliver siRNAs into cell lines or tissues. Naked siRNAs are unstable and are rapidly degraded, but PEI is able to form stable complexes with siRNAs, leading to the protection of genes from enzymatic degradation. Moreover, PEI shows a strong buffer capacity over a wide range of pH values; this plays an important role in the escape of genes from the endosome after endocytosis. On the other hand, the high cationic density of PEI allows for the formation of highly condensed complex with siRNAs, but complex formation with PEI can lead to cytotoxicity.[6–10] Information on the safety and biodistribution of PEI or PEI/siRNA complexes both in vitro and in vivo would contribute to improving the safety and efficiency of siRNA delivery using PEI.

In the present study, we introduced pullulan into PEI. Pullulan is a water-soluble polysaccharide consisting of three α-1,4-linked glucose polymers with different α-1,6-glucosidic linkages. It is used for liver targeting because of its high affinity for the asialoglycoprotein receptor in the liver.[11–13] We delivered PEI/siRNA or pullulan-containing PEI/siRNA complexes into mice through the tail vein by a hydrodynamics- or non-hydrodynamics-based injection. The incidence of mortality was found to increase with increasing the nitrogen/phosphorus (N/P) ratio of PEI/siRNA complexes. On the other hand, the introduction of pullulan into PEI reduced mouse mortality and increased liver-targeting efficiency.

2. Results and discussion

2.1. Polymers

A linear 22-kDa PEI was used for the synthesis of the siRNA and PEI-pullulan polymer complex (Fig. 1). The amount of pullulan in

* Corresponding author. Tel.: +81 6 6833 5012; fax: +81 6 6835 5476.
E-mail address: yamtet@ri.ncvc.go.jp (T. Yamaoka).
† These authors contributed equally to this work.

0968-0896/$ - see front matter © 2010 Elsevier Ltd. All rights reserved.
doi:10.1016/j.bmc.2010.04.031

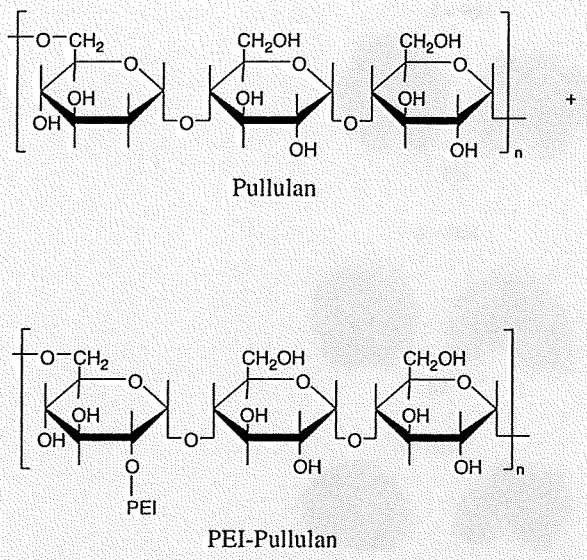

Figure 1. Chemical structure of pullulan and PEI-pullulan. To synthesize the PEI-pullulan polymer, 48.6 mg of pullulan (M_w, 107,000; 0.3 unit mmol) and 24.3 mg of carbonyldiimidazole (CDI; 0.15 mmol) were stirred in 30 mL of anhydrous dimethylsulfoxide (DMSO) at room temperature and then 13.2 mg of linear PEI (M_w, 22 kDa; 0.3 mmol) was added to the mixture.

the polymer was estimated to be 39 mol % and molecular weight of polymer was 2.6×10^5 (see Supplementary data). The zeta potentials of polymer/siRNA complex increased with increasing N/P ratio and showed nearly neutral at N/P ratios of 48 and 96 (see Supplementary data).

2.2. Measurements of complex diameters

The complexes of polymer and siRNA were prepared at several N/P ratios (1.5, 3, 6, 12, 24, and 48) and were determined using a Zetasizer. The particle size decreased with increasing N/P ratio. PEI/siRNA complexes showed <200 nm for all N/P ratios, whereas PEI-pullulan/siRNA complexes with ratios of 12 to 48 were <200 nm (Fig. 2).

2.3. Electrophoresis of the polymer/siRNA complex

Polymers were mixed with siRNA at several N/P ratios. The complexes were analyzed by electrophoresis. Bands corresponding

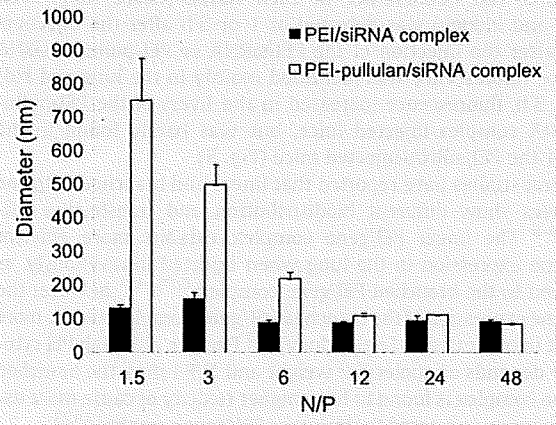

Figure 2. Diameter of the PEI/siRNA or PEI-pullulan/siRNA complexes. Polymer and siRNA complexes were simply prepared by incubating siRNA and polymer in water. The diameters of the complexes were determined using a Zetasizer.

Figure 3. Electrophoresis of (A) PEI/siRNA and (B) PEI-pullulan/siRNA complexes. Various concentrations of the polymer were mixed with the siRNA and analyzed by 19% polyacrylamide gel electrophoresis. A N/P ratio of 0 implies siRNA alone.

to free siRNA in the PEI/siRNA complex were not observed when the polymer was present at N/P ratios of above 3, whereas when the N/P ratios were 1.5 and 3, bands corresponding to free siRNA were observed. In the case of the PEI-pullulan/siRNA complex, no suppression of siRNA was indentified in those complexes with N/P ratios of 1.5 to 24, while siRNA migration in complexes with N/P ratios of $\geqslant$48 was suppressed (Fig. 3). These results show that introduction of pullulan into PEI weakens the polymer and siRNA complex.

2.4. Safety of polymer/siRNA complexes in vivo

PEI alone, the PEI/siRNA complex, and the PEI-pullulan/siRNA complex were injected into mice using a hydrodynamics-based or a non-hydrodynamics-based procedure. PEI alone or the PEI/siRNA complex with high N/P ratios ($\geqslant$6.0) increased mice mortality after systemic injection using the non-hydrodynamics-based procedure (Fig. 4); note that all mice died when complexes with N/P ratios of $\geqslant$12 were injected (data not shown). Similarly, previous studies reported that the PEI/DNA complex with a N/P ratio of 6 resulted in the death of 50% of the injected mice.[14,15] However, all mice died when PEI alone or the PEI/siRNA complex with a N/P ratio of 3 was injected using the hydrodynamics-based procedure. Hydrodynamics-based transfection was developed to deliver naked DNA or RNA into the liver by intravenous injection of a large volume of DNA or RNA solution at high velocity. This is an efficient method for liver-specific in vivo gene delivery.[16,17] However, in our study, high mouse mortality was observed when the hydrodynamics-based procedure was used for the in vivo delivery of PEI/siRNA complexes.

All dead mice lapsed into dyspnea less than 30 min after injection and showed hemorrhage-like dark red regions in the lung. There was no difference in mortality between mice injected with PEI alone and those injected with the PEI/siRNA complex, but more severe hemorrhage-like dark red regions were observed in the former (Fig. 4A and B).

Concerning the death of mice after systemic injection, Fahrmeir's group suggested that free PEIs after complex formation with DNA correlate with mouse mortality.[18] Several studies showed that increased gene expression in the lung is associated with lung damage and mouse mortality after intravenous injection of PEI/DNA or modified PEI/DNA.[15,19,20] In the present study, PEI/siRNA showed a similar in vivo toxicity to PEI/DNA.

On the other hand, no mortality was observed in mice injected with PEI-pullulan/siRNA complexes with N/P ratios of 6 to 48 by the hydrodynamics-based procedure mice (Fig. 4B) and the non-hydrodynamics-based procedure (data not shown). These

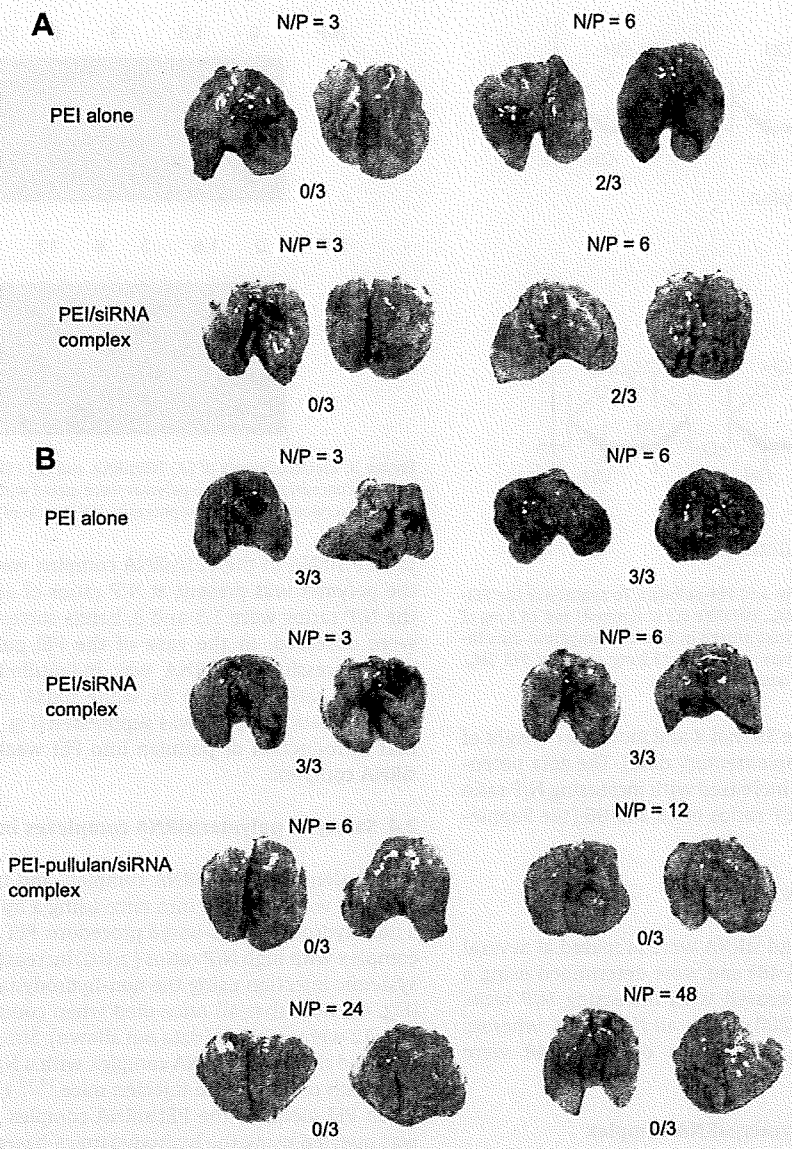

Figure 4. Delivery of PEI alone or polymer/siRNA complexes into mice by using the (A) non-hydrodynamics- or (B) hydrodynamics-based procedure. Numbers of dead mice per total mice are described below.

results suggest that intravenous injection with PEI alone or the PEI/siRNA complex at high N/P ratios can increase mortality, but introduction of pullulan into PEI results in low mortality. Moreover, hydrodynamics-based injection can increase the mouse mortality rate, compared to non-hydrodynamics-based injection. High in vivo toxicity or mortality caused by systemic injection of the PEI-based complex is an obstacle to be overcome. Many research efforts such as the introduction of poly(ethylene glycol) (PEG)[15] and removal of free PEIs after complex formation[18] were reported to efficiently reduce in vivo toxicity or mortality. In the present study, introduction of pullulan to PEI dramatically reduced in vivo toxicity and mortality.

2.5. Biodistribution after injection of the polymer/siRNA complex into mice

siRNA formed a complex with PEI at a N/P ratio of 3 and with PEI-pullulan at a N/P ratio of 48. Complexes were injected into the mice via the tail vein using the non-hydrodynamics-based procedure. The fluorescence in each tissue (heart, lung, liver, spleen, and kidney) was detected at 1 or 3 h after the injection. At 1 h after the injection of the PEI/siRNA or PEI-pullulan/siRNA complex, fluorescence was identified mainly in the lung and kidney. At 3 h, fluorescence increased in the livers of the PEI-pullulan/siRNA complex-injected mice, but was barely found in the livers of the PEI/siRNA-injected mice (Fig. 5).

Several studies have reported that linear and branched PEI/gene complexes show different biodistribution and transfection efficiency.[6–9] The linear PEI/gene complex exhibits more efficient transgene expression in the lung when injected intravenously, as compared to the branched PEI/gene complex;[6,7,9,14,21] however the transgene expression of the branched PEI/gene complex may be more efficient in other tissues (e.g., kidney).[9,22] Further, although PEI cytotoxicity depends on molecular weight and N/P ratios, the branched PEI/gene complex is found to have higher toxicity or cause more tissue damage as compared to the linear PEI/gene complex.[8,9,23]

In the present study, we used a linear 22-kDa PEI for complex formation with siRNA and for synthesizing the PEI-pullulan

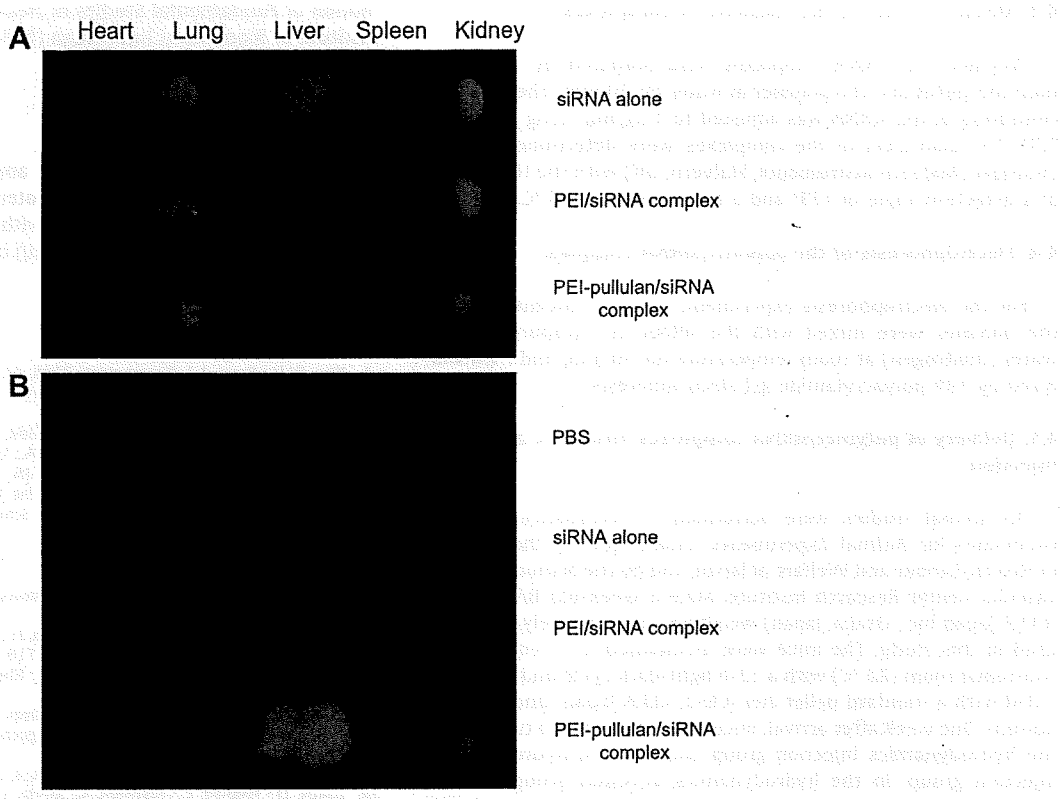

Figure 5. Biodistribution after injection of PBS, siRNA alone, or polymer/fluorescein-labeled siRNA complexes. The siRNA was bound with PEI at a N/P ratio of 3 and with PEI-pullulan at a N/P ratio of 48. The fluorescence in each tissue (heart, lung, liver, spleen, and kidney) was detected (A) 1 or (B) 3 h after the injection.

polymer. When the 22-kDa linear PEI/gene complexes were transfected via systemic administration, the main target was the lung and lower levels of transfection were found in the brain, heart, liver, spleen, and kidney.[14] High transgene expression in the lungs may relate to rapid crossing of the pulmonary endothelial barrier by the PEI/gene complexes.[21] Similarly, we found the highest level of fluorescence in the lung compared to other tissues (heart, liver, and spleen) at 1 h after intravenous injection of the PEI/siRNA complex at a N/P ratio of 3 (Fig. 5). Fluorescence in the kidney may be caused by elimination of biodegraded free fluorescein from the system.

siRNA-based therapeutics are recognized as a useful approach for liver (hepatic) diseases such as hepatitis B and C, but development of liver-targeted siRNA delivery system is an important problem to solve.[1] In the present study, pullulan, a water-soluble polysaccharide, was introduced into PEI to increase liver-targeting efficiency. At 3 h after the injection, we found highest level of fluorescence in the livers of the PEI-pullulan/siRNA complex-injected mice (Fig. 5). Thus, our system may be a useful means for efficient delivery of siRNA into the liver.

3. Conclusions

We found that introduction of pullulan to PEI increased the level of fluorescence in the liver. This finding may be explained by the fact that pullulan has a high affinity for asialoglycoprotein receptors in the liver.[11–13] Moreover, systemic delivery of PEI-pullulan polymer dramatically reduced mouse death. These results suggest that the PEI-pullulan polymer may be an efficient and low toxic means for siRNA delivery into the liver.

4. Materials and methods

4.1. Fluorescein-labeled siRNA

The gene (*apoB* siRNA) used in this study was amidated and its sequence was as follows: 5′-GUCAUCACACUGAAUACCAAUdTdT-3′ (sense) and 5′-dTdTCACAGUAGUGUGACUUAUGGUUA-3′ (antisense). Alexa Fluor 750 (Invitrogen, Tokyo, Japan) was used as an amine-reactive dye. The fluorescein-labeled siRNA was dialyzed against water containing 0.1% diethylpyrocarbonate (DEPC) for 2 days in a dialysis membrane bag with a molecular weight (MW) cut-off of 3500, followed by lyophilization.

4.2. Synthesis of PEI-pullulan polymer

A mixture of 48.6 mg of pullulan (M_w, 107,000; 0.3 unit mmol) and 24.3 mg of carbonyldiimidazole (CDI; 0.15 mmol) was stirred in 30 mL of anhydrous dimethylsulfoxide (DMSO) at room temperature. After 4 h, 13.2 mg of linear polyethyleneimine (PEI; M_w, 22 kDa; 0.3 mmol) was added to the mixture and further stirred at room temperature under a nitrogen-rich atmosphere for 1 day. The mixture was dialyzed against water for 3 days in a dialysis Spectra Pore membrane bag with a molecular weight cut-off of 10,000 (Spectrum Laboratories, Inc., Rancho Dominguez, CA), followed by lyophilization to obtain a PEI-pullulan polymer powder.

The buffering capacity of the PEI-pullulan polymer from pH 12 to 3 was determined by acid-base titration. Briefly, the polymer (4.8 mg) was dissolved in 8 mL of 150 mM NaCl to a final concentration of 0.6 mg/mL and the pH of the polymer solution was set to 12 with NaOH. The solution was subsequently titrated with 0.1 M HCl.